Long time horizons in optimal control: The turnpike property and asymptotic behavior of trajectories

Martin Gugat, Meizhi Qian, Jan Sokolowski

Long time horizons in optimal control: The turnpike property and asymptotic behavior of trajectories

Martin Gugat* Meizhi Qian* Jan Sokolowski†

Abstract

This paper investigates the dynamic turnpike phenomenon in Linear-Quadratic optimal control of abstract conservative systems governed by skew-adjoint operators with compact resolvents and bounded control operators. While classical turnpike theory emphasizes asymptotic convergence to a static steady state, this work focuses on characterizing the transient dynamics. We identify the *Initial Limit Arc* as the unique restriction of the infinite-horizon optimal trajectory to the stable invariant manifold of the Hamiltonian system. Exponential convergence of finite-horizon solutions to this limit arc is established in the energy norm, uniformly with respect to the time horizon. A spectral analysis of the decay rates reveals a fundamental dichotomy: the convergence exhibits either a control-dominated oscillatory regime or a saturation-limited monotonic regime, depending on the interplay between the regularization parameter and the principal eigenvalues. Numerical experiments on the wave equation and the Timoshenko beam system illustrate these regimes and verify the sharpness of the theoretical decay bounds.

Keywords: Turnpike property, Linear-quadratic optimal control problem, linear systems, dynamic optimal control problem, spectral methods, limit arcs

1 Introduction

Optimal control problems governed by partial differential equ-ations (PDEs) constitute a canonical class of infinite-dimensional optimization challenges. Within this broad scope, the Linear–Quadratic (LQ) formulation serves as the standard paradigm [20, 5, 32]. This framework is grounded in classical theories of Riccati equations, including foundational results for hyperbolic dynamics with L_2-Dirichlet boundary terms [18], providing a unified analytical framework that accommodates systems exhibiting both parabolic and hyperbolic characteristics [27, 34, 36, 11].

However, despite the universality of this classical theory, its analytical foundation is not fully developed when applied to conservative hyperbolic dynamics. The core difficulty lies in the absence of intrinsic dissipation. Specifically, in parabolic settings, the solution to the algebraic Riccati equation typically exhibits a smoothing property, mapping the state space into a subspace of higher regularity. This intrinsic regularization naturally suppresses high-frequency modes, facilitating the proof of turnpike convergence. In contrast, for conservative systems governed by skew-adjoint generators, the Riccati operator remains strictly bounded on the energy space and lacks this compact smoothing action. Understanding the regularity of such systems often requires analyzing subtle properties, such as the hidden boundary regularity for wave equations with mixed boundary conditions [3]. As a result, the high-frequency oscillatory structure of the state is preserved under feedback, rendering standard regularization-based arguments ineffective. To analyze the asymptotic behavior despite this lack of dissipation-induced smoothing, we adopt a direct spectral decomposition approach. Rather than relying on the regularization of the Riccati operator, this framework allows us to explicitly resolve the competition between control damping and conservative oscillations mode-by-mode. While recent developments have addressed turnpike phenomena in conservative settings [33, 12], these results predominantly rely on averaged estimates (integral turnpike) and do not resolve the precise pointwise-in-time

*Friedrich-Alexander-Universität Erlangen-Nürnberg, Department of Mathematics, Lehrstuhl für Dynamics, Control, Machine Learning and Numerics (Alexander von Humboldt-Professur), Cauerstr. 11, 91058 Erlangen, Germany.

†Institut Élie Cartan de Lorraine, CNRS, UMR 7502, Université de Lorraine, B.P. 70239, 54506 Vandoeuvre-lès-Nancy Cedex, France; Systems Research Institute of the Polish Academy of Sciences, ul. Newelska 6, 01-447 Warszawa, Poland; Department of Scientific Computing, Informatics Center, Federal University of Paraiba, Brazil.

structure of the optimal trajectory. For discrete-time and continuous-time settings, a comprehensive overview of turnpike properties and their connection to strict dissipativity has been provided in [9, 10]. These works highlight the role of control cost in determining convergence regimes and provide rigorous bounds for the transient dynamics of optimal trajectories.

A particularly challenging subclass arises when the dynamics are governed by abstract second-order evolution equations generated by skew-adjoint operators with compact resolvents [35, 25, 8]. This operator-theoretic framework canonically realizes classical conservative models, including the wave equation and coupled hyperbolic systems such as the Timoshenko beam [21, 17]. The defining feature of these systems is their purely imaginary spectrum, which eliminates any form of analytic smoothing. In contrast to dissipative dynamics—where high-frequency modes are naturally attenuated—conservative systems sustain oscillatory behavior at all frequencies, and these oscillations interact nontrivially with the control input. As a result, the optimal state cannot relax toward the steady-state minimizer through natural damping; instead, it must evolve along an invariant spectral subspace dictated by the optimality system. This evolution is controlled by a interplay between the regularization weight in the cost functional and the intrinsic oscillatory modes of the generator, producing a transient phase whose structure resists characterization by standard approaches.

Despite significant advances in the study of turnpike phenomena, the conservative setting still lacks a pointwise-in-time spectral framework capable of resolving the fine structure of the initial boundary layer under optimal control feedback. Classical semigroup techniques, while sufficient for establishing well-posedness and qualitative stability [31], offer limited insight into how the optimality system couples and redistributes modal energy during the initial stage of the evolution. Likewise, spectral inequalities and microlocal observability estimates provide sharp but inherently global bounds [6, 19, 4], rendering them incapable of capturing the transient, mode-by-mode competition between control penalization and intrinsic system dynamics. Crucially, existing theory does not fully describe the mode-dependent redistribution of energy that governs the transition from the initial state to the turnpike regime. These limitations highlight the necessity of a spectral perspective—one that isolates and characterizes the dynamics of individual eigenmodes to uncover the mechanism driving the conservative turnpike transition.

In this work, we develop such a framework by providing a rigorous long-horizon analysis of LQ optimal control problems for abstract second-order evolution equations. Our central objective is to obtain a pointwise-in-time, mode-resolved characterization of the initial transient dynamics, thereby extending beyond the integral-averaged descriptions typically available in the literature [15, 12, 14]. Using the spectral decomposition of the conservative generator, we explicitly resolve the Hamiltonian optimality system [7] and uncover a diagonal block structure that remains inaccessible through classical PDE-based methods. This structural insight enables us to rigorously identify the initial layer as a well-defined dynamic trajectory—termed the Initial Limit Arc—which admits an explicit parametrization in terms of the principal eigenfrequencies. This construction provides a precise analytical description of the transient phase and reveals a fundamental spectral dichotomy: a transition from control-dominated to saturation-limited decay rates, which ultimately governs the exponential convergence toward the turnpike [2, 1].

The main contributions of this paper are summarized as follows:

1. Construction of the Initial Limit Arc: We rigorously establish the existence and uniqueness of the Initial Limit Arc, a dynamic trajectory that governs the optimal transition from the initial state in the infinite-horizon limit. Complementing classical turnpike theory—which typically characterizes convergence to a static steady state or its associated infinite-horizon trajectory—we identify this limit arc as the unique solution of the infinite-horizon optimality system residing on the stable invariant manifold, explicitly resolving the transient trajectory typically described only via its asymptotic limit.

2. Uniform Exponential Convergence Estimates: We prove that the finite-horizon optimal state converges to the Initial Limit Arc exponentially fast in the energy topology. By employing a spectral decomposition approach under a spectral gap assumption, we derive uniform estimates with respect to the time horizon.

3. Spectral Dichotomy of Decay Rates: We provide a spectral analysis of the convergence rate, revealing a distinct transition determined by the interplay between the regularization parameter and the principal eigenvalue. We distinguish between a control-dominated oscillatory regime and a saturation-limited monotonic regime, demonstrating that the decay rate is bounded by the system's intrinsic dynamics as the control cost vanishes.

4. Numerical Verification on Coupled Hyperbolic Systems: We employ an adjoint-based discrete optimization scheme to validate the theoretical estimates on the 1D and 2D wave equations and the Timoshenko beam model. The results show that the empirical decay of the error consistently conforms to the spectral predictions in both convergence regimes.

The paper is organized as follows. Section 2 establishes the abstract operator-theoretic framework, instantiated by the wave equation and the Timoshenko beam model. The asymptotic analysis follows in Section 3, where we construct the Initial Limit Arc and derive uniform convergence rates. Section 4 details the numerical methodology, including the adjoint-based discrete optimization. Experimental validation on 1D and 2D systems is presented in Section 5. Finally, Section 6 offers concluding remarks, with technical proofs deferred to Appendix A.

2 Mathematical Formulation and Abstract Framework

This section establishes a rigorous operator-theoretic framework for the optimal control problem. First, we introduce an abstract first-order evolution equation governed by a skew-adjoint generator. Subsequently, we demonstrate that the specific second-order mechanical systems of interest—namely, the wave equation and the Timoshenko beam—serve as canonical realizations of this abstract framework within an appropriate energy space. This unified approach allows us to exploit the spectral properties of the generator to analyze the turnpike phenomenon [35].

2.1 The Abstract First-Order System

Let $\mathcal{X}$ and U be separable Hilbert spaces, representing the state space and the control space, respectively. Consider a linear dynamical system governed by the abstract first-order evolution equation:

$$\begin{cases} \dot{z}(t) = \mathcal{A}z(t) + \mathcal{B}u(t), \quad t \in (0,T), \\ z(0) = z_0, \end{cases} \tag{1}$$

where $z(t) \in \mathcal{X}$ is the state trajectory, $u \in L^2(0,T;U)$ is the control input, and $z_0 \in \mathcal{X}$ is the initial datum.

The well-posedness and asymptotic properties of the system rely fundamentally on the spectral structure of the operator $\mathcal{A}$. We impose the following assumptions, which are characteristic of conservative wave-like systems.

Assumption 1 (Skew-Adjoint Generator)**.** *The operator $\mathcal{A} : \mathcal{D}(\mathcal{A}) \subset \mathcal{X} \to \mathcal{X}$ is a linear, unbounded, and densely defined operator. We assume that:*

1. *$\mathcal{A}$ is* skew-adjoint*, i.e., $\mathcal{A}^* = -\mathcal{A}$.*
2. *The operator has a compact resolvent, specifically, $0 \in \rho(\mathcal{A})$ and the inverse $\mathcal{A}^{-1}$ is a compact operator on $\mathcal{X}$.*

Consequently, the spectrum $\sigma(\mathcal{A})$ consists exclusively of isolated purely imaginary eigenvalues. According to Stone's Theorem, $\mathcal{A}$ generates a strongly continuous group of unitary operators $(\mathbb{T}_t)_{t\in\mathbb{R}}$ on $\mathcal{X}$. This implies that the unforced system ($u \equiv 0$) is conservative, satisfying the energy identity:

$$\|z(t)\|_{\mathcal{X}} = \|z_0\|_{\mathcal{X}}, \quad \forall t \geq 0. \tag{2}$$

Assumption 2 (Admissible Control)**.** *The control operator $\mathcal{B}$ is a bounded linear operator, satisfying $\mathcal{B} \in \mathcal{L}(U, \mathcal{X})$.*

Under Assumptions 1 and 2, for any initial state $z_0 \in \mathcal{X}$ and control input $u \in L^2(0,T;U)$, the unique mild solution to 1 is given by Duhamel's formula:

$$z(t) = \mathbb{T}_t z_0 + \int_0^t \mathbb{T}_{t-s}\mathcal{B}u(s)\,\mathrm{d}s. \tag{3}$$

The finite-horizon objective functional $J_T : L^2(0,T;U) \to \mathbb{R}$ is defined as

$$J_T(u) := \frac{1}{2}\int_0^T \left(\|z(t) - z_d\|_{\mathcal{X}}^2 + \gamma\|u(t)\|_U^2\right) \mathrm{d}t. \tag{4}$$

Without loss of generality, we assume the target state is the zero equilibrium, $z_d = 0$. The dynamic optimal control problem is formulated as:

$$\min_{u\in L^2(0,T;U)} J_T(u) \quad \text{subject to (1).} \tag{OCP$_T$}$$

Since the cost functional J_T is strictly convex and coercive, standard theory guarantees the existence and uniqueness of an optimal control u_T^*.

Remark 1. *While Assumption 2 focuses on bounded control operators (canonical for distributed control), this choice is strategic rather than restrictive. The fundamental challenge in extending the turnpike theory to conservative systems lies in the absence of intrinsic dissipation and the resulting persistence of oscillatory modes across the entire spectrum. Unlike parabolic systems where natural damping facilitates stabilization, conservative dynamics require the control input to actively reshape the energy distribution of the trajectory. By considering bounded operators, we isolate this dynamical challenge from the regularity singularities associated with unbounded boundary actuation. This setting allows for a rigorous characterization of the Initial Limit Arc and uncover the spectral dichotomy between the control-dominated and saturation-limited regimes—phenomena that are intrinsic to the skew-adjoint generator $\mathcal{A}$ and independent of the specific realization of $\mathcal{B}$. Consequently, the results presented here establish the fundamental asymptotic structure for conservative control problems, serving as the requisite baseline for future extensions to boundary control scenarios involving admissibility criteria [35].*

2.2 Application to Second-Order Hyperbolic Systems

This subsection specializes the abstract framework to general second-order evolution equations, showing that they constitute a canonical realization of the first-order system 1.

Let H be a separable real Hilbert space and let $A_0 : \mathcal{D}(A_0) \subset H \to H$ be a self-adjoint, positive-definite operator with a compact inverse. We consider the second-order system:

$$y_{tt}(t) + A_0 y(t) = B_0 u(t), \quad y(0) = y_0, \quad y_t(0) = 0, \tag{5}$$

where $B_0 \in \mathcal{L}(U, H)$ denotes the control operator.

The reduction to the first-order form 1 is achieved on the energy space $\mathcal{X} := \mathcal{D}(A_0^{1/2}) \times H$, explicitly equipped with the inner product:

$$\langle (v_1, h_1), (v_2, h_2)\rangle_{\mathcal{X}} := \langle A_0^{1/2} v_1, A_0^{1/2} v_2\rangle_H + \langle h_1, h_2\rangle_H. \tag{6}$$

By introducing the state vector $z(t) := (y(t), y_t(t))^\top$, the system operator $\mathcal{A}$ and the lifted control operator $\mathcal{B}$ are defined via the block matrices:

$$\mathcal{A} = \begin{pmatrix} 0 & I \\ -A_0 & 0 \end{pmatrix}, \quad \mathcal{B} = \begin{pmatrix} 0 \\ B_0 \end{pmatrix}, \tag{7}$$

with the domain $\mathcal{D}(\mathcal{A}) = \mathcal{D}(A_0) \times \mathcal{D}(A_0^{1/2})$. This construction is classical in the theory of conservative systems and is recalled here for completeness.

Proposition 1. *The operator $\mathcal{A}$ defined above is skew-adjoint on the energy space $\mathcal{X}$.*

Proof. The skew-symmetry of $\mathcal{A}$ follows directly from the definition of the inner product in 6, where the terms $\langle A_0 v, h\rangle_H$ and $\langle h, -A_0 v\rangle_H$ cancel out. The surjectivity of $\mathcal{A}$ (and hence skew-adjointness) is a consequence of the invertibility of A_0, which is ensured by its positive definiteness. We refer to [35, Proposition 3.7.6] for detailed derivations. □

2.2.1 Model Problem I: The Wave Equation

The first concrete instance of our framework concerns the distributed control of the classical wave equation. Let $\Omega \subset \mathbb{R}^n$ $(n \geq 1)$ be a bounded domain with sufficiently smooth boundary $\partial\Omega$.

To align with the abstract setting, the state space is chosen as $H = L^2(\Omega)$ and the control space as $U = L^2(\Omega)$. The spatial operator is the Dirichlet Laplacian $A_0 = -\Delta$ with domain $\mathcal{D}(A_0) = H^2(\Omega) \cap H_0^1(\Omega)$, so that the energy space $V = \mathcal{D}(A_0^{1/2})$ coincides with $H_0^1(\Omega)$, equipped with the gradient norm $\|v\|_V = \|\nabla v\|_{L^2}$.

Let $Q_T := (0,T) \times \Omega$ denote the space-time cylinder and $\Sigma_T := (0,T) \times \partial\Omega$ its lateral boundary. The state trajectory $y \in C([0,T];V) \cap C^1([0,T];H)$ satisfies

$$\begin{cases} \partial_{tt} y - \Delta y = u & \text{in } Q_T, \\ y = 0 & \text{on } \Sigma_T, \\ y(0) = y_0 \in V, \quad \partial_t y(0) = 0 & \text{in } \Omega. \end{cases} \tag{8}$$

The control operator $B_0 : U \to H$ is the identity embedding. Given a target profile $y_d \in V$, the tracking functional is

$$J_T^{\text{wave}}(y,u) := \frac{1}{2} \int_0^T \int_\Omega \left(|\partial_t y|^2 + |\nabla(y - y_d)|^2 + \gamma |u|^2 \right) \mathrm{d}x\mathrm{d}t, \tag{9}$$

with regularization parameter $\gamma > 0$. Minimizing 9 subject to 8 is equivalent to the abstract problem (OCP_T) with block operators $\mathcal{A}$ and $\mathcal{B}$ defined in Section 2, and target state $z_d = (y_d, 0)^\top$. The term $|\partial_t y|^2 + |\nabla(y - y_d)|^2$ in the integral coincides with the abstract energy norm in $\mathcal{X} = H_0^1(\Omega) \times L^2(\Omega)$. Zero initial velocity is assumed; the extension to general initial data is straightforward.

2.2.2 Model Problem II: The Timoshenko Beam System

The framework naturally extends to coupled vector-valued dynamics, exemplified by the Timoshenko beam. Let $\Omega = (0, L)$ denote the beam span, and define the state vector $\boldsymbol{y}(t,x) := (w(t,x), \varphi(t,x))^\top$, representing vertical displacement and rotation angle. The dynamics on $Q_T = (0,T) \times \Omega$ satisfy

$$\begin{cases} \rho w_{tt} - K(w_{xx} - \varphi_x) = f, \\ I_\rho \varphi_{tt} - EI\varphi_{xx} - K(w_x - \varphi) = m, \end{cases} \tag{10}$$

with clamped boundary conditions $w = \varphi = 0$ at $x \in \{0, L\}$, initial displacement $\boldsymbol{y}(0) = \boldsymbol{y}_0$, and zero initial velocity. The distributed control input is $\boldsymbol{u} = (f, m)^\top$.

To match the abstract second-order form $\boldsymbol{y}_{tt} + A_0 \boldsymbol{y} = B_0 \boldsymbol{u}$, we introduce the weighted Hilbert space

$$H := L^2_\rho(\Omega) \times L^2_{I_\rho}(\Omega), \quad \langle \boldsymbol{y}, \tilde{\boldsymbol{y}} \rangle_H := \int_0^L (\rho w \tilde{w} + I_\rho \varphi \tilde{\varphi}) \, \mathrm{d}x, \tag{11}$$

where $\rho > 0$ is the mass density, $I_\rho > 0$ the rotational inertia, $EI > 0$ the bending stiffness, and $K > 0$ the shear stiffness. The control operator $B_0 : L^2(\Omega)^2 \to H$ is the identity embedding. The spatial operator $A_0 : \mathcal{D}(A_0) \subset H \to H$ is given by

$$A_0 \boldsymbol{y} = \begin{pmatrix} -\frac{K}{\rho}(w_{xx} - \varphi_x) \\ -\frac{EI}{I_\rho}\varphi_{xx} - \frac{K}{I_\rho}(w_x - \varphi) \end{pmatrix}, \quad \mathcal{D}(A_0) = (H^2(\Omega) \cap H_0^1(\Omega))^2, \tag{12}$$

ensuring that A_0 is self-adjoint and positive-definite on H.

The cost functional reflecting total mechanical energy is

$$J_T^{\text{beam}}(\boldsymbol{y}, \boldsymbol{u}) := \frac{1}{2} \int_0^T \left(\|\boldsymbol{y}_t\|_H^2 + \langle A_0(\boldsymbol{y} - \boldsymbol{y}_d), \boldsymbol{y} - \boldsymbol{y}_d \rangle_H + \gamma \|\boldsymbol{u}\|_{L^2}^2 \right) \mathrm{d}t. \tag{13}$$

Here, $\gamma > 0$ is the regularization parameter. Noting that $\langle A_0 \cdot, \cdot \rangle_H$ defines the squared norm in $V = \mathcal{D}(A_0^{1/2})$, this problem is strictly equivalent to the abstract objective 4 with block operators $\mathcal{A}$ and $\mathcal{B}$ from Section 2.1, ensuring full consistency with the abstract framework (OCP_T).

3 Asymptotic Analysis and the Initial Limit Arc

This section investigates the asymptotic behavior of the optimal state trajectory $y_T(t)$ as the time horizon $T \to \infty$. While the system dynamics are governed by the abstract generator $\mathcal{A}$ defined in Section 2, the turnpike phenomenon is analyzed here using the spectral decomposition of the spatial operator A_0. This mode-wise decomposition allows for a precise characterization of the convergence rates and the dichotomy between oscillatory and monotonic regimes. Let $\{\varphi_j\}_{j\in\mathbb{N}}$ be the orthonormal eigenbasis of A_0 in H, with corresponding eigenvalues $0 < \lambda_1 \le \lambda_2 \le \cdots < \infty$. The state $y(t)$ admits the expansion:

$$y(t) = \sum_{j=1}^{\infty} \alpha_j(t)\varphi_j. \tag{14}$$

The limit trajectory, referred to as the *Initial Limit Arc* and denoted by $\Xi(t)$, is identified as the solution to the infinite-horizon problem residing on the stable manifold. The main result establishes that the finite-horizon optimal trajectory $y_T(t)$ converges to this infinite-horizon limit $\Xi(t)$ exponentially fast in the energy topology $V = \mathcal{D}(A_0^{1/2})$.

The asymptotic behavior is dictated by the roots of the characteristic polynomial associated with the j-th mode optimality system:

$$p_j(s) := s^4 + (2\lambda_j - \gamma^{-1})s^2 + \lambda_j(\lambda_j + \gamma^{-1}). \tag{15}$$

Assumption 3. *Let $\mathcal{S} := \bigcup_{j\in\mathbb{N}}\{s \in \mathbb{C} \mid p_j(s) = 0\}$ denote the set of all characteristic roots. It is assumed that a global spectral gap $\mu > 0$ exists:*

$$\mu := \inf_{s\in\mathcal{S}} |\mathrm{Re}(s)| > 0. \tag{16}$$

Remark 2. *The spectral gap condition $\mu > 0$ in Assumption 3 acts as the crucial generator for the uniform exponential decay estimates established later in Theorem 1. We note that this condition requires the real parts of the characteristic roots to be bounded away from zero, which is distinct from requiring strict separation of the spatial eigenvalues λ_j. In multi-dimensional domains, while λ_j may cluster, the asymptotic behavior $\lambda_j \to \infty$ (Weyl's Law) ensures that the high-frequency roots of $p_j(s)$ maintain a non-vanishing real part. Consequently, the global gap μ remains strictly positive for the bounded domains considered here, provided the high-frequency modes do not accumulate on the imaginary axis (a property ensured by the discrete spectrum of $\mathcal{A}$ on bounded domains).*

However, it is insightful to consider the loss of this gap. In unbounded domains or singular geometries, the spectrum becomes continuous, potentially leading to $\mu \to 0$. In such regimes, the exponential decay is expected to degenerate into polynomial convergence. Our framework thus focuses on the discrete spectral regime, establishing the requisite baseline for future extensions to infinite-energy settings.

Definition 1 (Initial Limit Arc)**.** *The Initial Limit Arc, denoted by $\Xi(\cdot)$, is defined as the unique solution to the infinite-horizon optimality system satisfying the initial condition $\Xi(0) = y_0$ and the finite energy constraint $\Xi \in L^2(0,\infty;V)$.*

From a dynamical systems perspective, $\Xi(t)$ corresponds to the trajectory evolving strictly on the stable invariant manifold of the associated Hamiltonian operator. Consistent with classical turnpike theory, it serves as a dynamic turnpike attractor: as the horizon $T \to \infty$, the finite-horizon optimal state $y_T(t)$ does not converge to a static point but rather exponentially tracks $\Xi(t)$ during the initial transient phase, deviating only as the terminal boundary layer becomes dominant.

Theorem 1 (Global Exponential Convergence)**.** *Let $y_0 \in V$ be the initial state. Under Assumption 3, the Initial Limit Arc Ξ (defined in Definition 1) satisfies the regularity property $\Xi \in C([0,\infty);V)$. Furthermore, the finite-horizon optimal state $y_T(t)$ of problem (OCP_T) converges to $\Xi(t)$ with the following properties:*

1. ***Pointwise Convergence:*** *For any fixed time $t \ge 0$, the finite-horizon optimal state converges to the limit trajectory:*

$$\lim_{T\to\infty} \|y_T(t) - \Xi(t)\|_V = 0. \tag{17}$$

2. ***Uniform Exponential Convergence:*** *The convergence is exponentially fast and uniform with respect to the horizon. There exists a constant $C > 0$ independent of T such that:*

$$\|y_T(t) - \Xi(t)\|_V \leq C \|y_0\|_V e^{-\mu(T-t)}, \quad \forall t \in [0, T). \tag{18}$$

The decay rate μ is strictly positive and characterized by a spectral dichotomy involving the regularization parameter γ and the principal eigenvalue λ_1:

   (a) *Oscillatory Regime: If $\lambda_1 > \frac{1}{8\gamma}$, the convergence is oscillatory with rate $\mu \geq \frac{1}{2\sqrt{\gamma}}$.*

   (b) *Monotonic Regime: If $\lambda_1 \leq \frac{1}{8\gamma}$, the convergence is monotonic (overdamped) with rate $\mu \geq \mathrm{Re}(\sqrt{\lambda_1})$.*

Consequently, the global decay rate satisfies the uniform lower bound:

$$\mu \geq \min\left(\frac{1}{2\sqrt{\gamma}}, \mathrm{Re}(\sqrt{\lambda_1})\right). \tag{19}$$

3. ***Exponential Stability of the Limit Arc:*** *The limit arc $\Xi(t)$ itself decays exponentially to the target steady state $y_d = 0$ as $t \to \infty$:*

$$\|\Xi(t) - y_d\|_V = \|\Xi(t)\|_V \leq Ce^{-\mu t}. \tag{20}$$

Proof of Theorem 1. The proof proceeds via the spectral decomposition of the spatial operator A_0. By projecting the system dynamics onto the orthonormal eigenbasis $\{\varphi_j\}_{j\in\mathbb{N}}$, the infinite-dimensional optimization problem decouples into a sequence of independent scalar fourth-order problems. The convergence analysis is subsequently performed mode-by-mode. For brevity, the explicit analytical construction of the coefficients and detailed algebraic verifications are provided in Appendix A.

Step 1: Modal Decomposition and Optimality System. Let $y_0 = \sum_{j=1}^{\infty} \eta_j \varphi_j$ be the expansion of the initial state. The condition $y_0 \in V$ implies $\sum_{j=1}^{\infty} \lambda_j |\eta_j|^2 < \infty$. Consistent with the target state $y_d = 0$, the target coefficients are zero ($\beta_j = 0$).

Substituting the modal expansion $y(t) = \sum \alpha_j(t)\varphi_j$ and the dynamics relation $u_j(t) = \alpha_j''(t) + \lambda_j \alpha_j(t)$ into the cost functional yields the decoupled objective:

$$J_T(y, u) = \sum_{j=1}^{\infty} \int_0^T \left(|\alpha_j'(t)|^2 + \lambda_j |\alpha_j(t)|^2 + \gamma |\alpha_j''(t) + \lambda_j \alpha_j(t)|^2\right) \, \mathrm{d}t.$$

directly leads to the Euler-Lagrange equation for the optimal coefficient $\alpha_j(T; t)$. The resulting fourth-order ODE is homogeneous:

$$\alpha_j^{(4)} + \left(2\lambda_j - \frac{1}{\gamma}\right) \alpha_j^{(2)} + \lambda_j \left(\lambda_j + \frac{1}{\gamma}\right) \alpha_j = 0, \tag{21}$$

subject to the initial conditions $\alpha_j(0) = \eta_j$, $\alpha_j'(0) = 0$ and the terminal transversality conditions at $t = T$:

$$\alpha_j''(T) = -\lambda_j \alpha_j(T), \quad \alpha_j'''(T) = \left(\frac{1}{\gamma} - \lambda_j\right) \alpha_j'(T).$$

The characteristic polynomial associated with 21 is $p_j(s) = s^4 + (2\lambda_j - \gamma^{-1})s^2 + \lambda_j(\lambda_j + \gamma^{-1})$. Setting $\zeta = s^2$, the discriminant is given by

$$\Delta_j = \frac{1}{\gamma}(\frac{1}{\gamma} - 8\lambda_j).$$

This partitions the spectrum $\mathbb{N}$ into two distinct regimes:

1. Oscillatory Modes (I_{osc}): $\Delta_j < 0$ (i.e., $\lambda_j > \frac{1}{8\gamma}$). The roots are complex quartets $\pm\omega_j, \pm\bar{\omega}_j$.

2. Monotonic Modes (I_{mono}): $\Delta_j \geq 0$ (i.e., $\lambda_j \leq \frac{1}{8\gamma}$). The roots are real pairs $\pm\rho_{j,1}, \pm\rho_{j,2}$.

Step 2: Analysis of Characteristic Roots and Spectral Gap. The asymptotic behavior is governed by the location of the roots of the characteristic equation $p_j(s) = 0$. We analyze the two regimes dictated by the discriminant Δ_j:

1. Oscillatory Regime ($j \in I_{osc}$): For modes with $\lambda_j > (8\gamma)^{-1}$, the roots form complex quartets. Let ω_j denote the stable root in the second quadrant. The real and imaginary parts satisfy:

$$|\mathrm{Re}(\omega_j)| \geq \frac{1}{2\sqrt{\gamma}} \quad \text{and} \quad \lim_{j\to\infty} |\mathrm{Im}(\omega_j)| = \infty. \tag{22}$$

The strictly positive lower bound on the real part implies that the decay rate for high-frequency modes is limited by the control regularization parameter γ, independent of the frequency j.

2. Monotonic Regime ($j \in I_{mono}$): For finite modes with $\lambda_j \leq (8\gamma)^{-1}$, the roots are real and negative. As detailed in Appendix A, the slowest decaying root scales as $\sqrt{\lambda_j}$.

Combining both regimes, the global spectral gap is uniform:

$$\mu := \inf_{j\in\mathbb{N}} |\mathrm{Re}(z_j)| \geq \min\left(\frac{1}{2\sqrt{\gamma}}, \mathrm{Re}(\sqrt{\lambda_1})\right) > 0. \tag{23}$$

This uniform gap μ is the key generator of the exponential convergence established in Theorem 1. The explicit algebraic construction of the finite-horizon solution $\alpha_j(T;t)$ and its coefficients are deferred to Appendix A.

Step 3: Rigorous Construction of the Initial Limit Arc. The objective is to characterize the limit trajectory $\Xi_j(t)$ describing the asymptotic evolution near the initial time. Mathematically, $\Xi_j(t)$ corresponds to the unique solution of the modal optimality system on the infinite interval $[0, \infty)$.

The condition of finite cost requires $\Xi_j \in L^2(0,\infty)$, which implies that $\Xi_j(t)$ must reside strictly on the stable manifold. Thus, it admits the general structural form:

$$\Xi_j(t) = c_{j,1}e^{\nu_{j,1}t} + c_{j,2}e^{\nu_{j,2}t}, \tag{24}$$

where $\nu_{j,1}, \nu_{j,2}$ denote the stable characteristic roots satisfying $\mathrm{Re}(\nu_{j,k}) \leq -\mu < 0$. The coefficients $c_{j,k}$ are uniquely determined by the initial conditions $\Xi_j(0) = \eta_j$ and $\Xi_j'(0) = 0$. This structure highlights the spectral dichotomy:

1. Oscillatory Regime ($j \in I_{osc}$): The roots are complex conjugates $\nu_{j,1} = \omega_j, \nu_{j,2} = \bar{\omega}_j$, leading to damped oscillations.

2. Monotonic Regime ($j \in I_{mono}$): The roots are real and negative, leading to overdamped, monotonic decay.

We now identify the specific coefficients $c_{j,k}$ by computing the pointwise limit of the finite-horizon solution $\alpha_j(T;t)$ as $T \to \infty$. Let $\mu_j = |\mathrm{Re}(\omega_j)|$. Since the unstable modes grow as $|\cosh(\omega_j T)| \sim \frac{1}{2}e^{\mu_j T}$, we analyze the ratio of the numerator to the denominator $N_j(T)$.

The denominator scales as (see Appendix A for coefficients):

$$\lim_{T\to\infty} \frac{N_j(T)}{e^{2\mu_j T}} = \frac{1}{4}\left[|\omega_j|^2\left(\frac{4\lambda_j}{\gamma} - \gamma^{-2}\right) + \lambda_j\left(\frac{4\lambda_j}{\gamma} + \gamma^{-2}\right)\right] := g_j. \tag{25}$$

In the numerator, terms with repeated frequency indices (e.g., $\cosh(\omega_j T)\cosh(\omega_j(T-t))$) scale at a rate strictly lower than $e^{2\mu_j T}$ due to algebraic cancellation, and thus vanish in the limit. Consequently, the surviving contributions arise exclusively from the *dominant cross-terms* between distinct stable roots. Applying the limit identity:

$$\lim_{T\to\infty} e^{-2\mu_j T}\cosh(\omega_j T)\cosh(\bar{\omega}_j(T-t)) = \frac{1}{4}e^{\bar{\omega}_j t}, \tag{26}$$

we derive the explicit pointwise limit:

$$\Xi_j(t) := \lim_{T\to\infty} \alpha_j(T;t) = \frac{1}{2}\frac{\eta_j}{g_j}\mathrm{Re}\left([\mathcal{C}_1 - \mathcal{C}_2]e^{\bar{\omega}_j t}\right). \tag{27}$$

Simplifying the constants matches the abstract form (24) specifically with:

$$\Xi_j(t) = \eta_j L_j(t), \quad \text{with} \quad L_j(t) := \mathrm{Re}\left(\frac{\bar{\omega}_j e^{\omega_j t} - \omega_j e^{\bar{\omega}_j t}}{\bar{\omega}_j - \omega_j}\right). \tag{28}$$

This explicitly confirms that the finite-horizon solution converges pointwise to the unique stable manifold trajectory defined by the initial data η_j. Since $\mathrm{Re}(\omega_j) \leq -\mu$, Eq. (28) guarantees the exponential decay

$$|\Xi_j(t)| \leq C_j|\eta_j|e^{-\mu t}. \tag{29}$$

Step 4: Convergence in the Energy Norm. The finite-horizon solution $\alpha_j(T;t)$ differs from the infinite-horizon limit $\Xi_j(t)$ due to boundary layer terms reflecting from $t = T$. Detailed asymptotic analysis (Appendix A) yields the uniform estimate:

$$|\alpha_j(T;t) - \Xi_j(t)| \leq K|\eta_j|e^{-\mu(T-t)}. \tag{30}$$

Reconstructing the global error in the energy topology by summing over all eigenmodes yields:

$$\|y_T(t) - \Xi(t)\|_V^2 = \sum_{j=1}^{\infty} \lambda_j |\alpha_j(T;t) - \Xi_j(t)|^2 \leq K^2 e^{-2\mu(T-t)} \sum_{j=1}^{\infty} \lambda_j |\eta_j|^2. \tag{31}$$

Identifying the series $\sum_{j=1}^{\infty} \lambda_j|\eta_j|^2$ as the squared initial energy $\|y_0\|_V^2$, we derive the global uniform estimate:

$$\|y_T(t) - \Xi(t)\|_V \leq C \|y_0\|_V e^{-\mu(T-t)}, \quad \text{with } C = K. \tag{32}$$

This estimate strictly verifies the exponential convergence rate asserted in Eq. (18) of Theorem 1. Furthermore, by fixing t and letting $T \to \infty$, the right-hand side vanishes, thereby rigorously establishing the pointwise convergence claimed in Eq. (17).

□

Remark 3. *The theoretical dichotomy predicts that as $\gamma \to 0$, the convergence rate does not increase indefinitely but saturates at the system's natural frequency $Re(\sqrt{\lambda_1})$. This saturation effect explains the specific decay limits observed in the numerical experiments (Section 5).*

4 Optimality System and Discretization

This section establishes the necessary optimality conditions for the infinite-dimensional problem (OCP_T) and introduces a consistent discretization strategy. Consistent with the asymptotic analysis in Section 3, we analyze (OCP_T) as the finite-horizon formulation asymptotically consistent with the infinite-horizon problem that defines the Initial Limit Arc. A standard "first optimize, then discretize" approach is adopted: the Karush-Kuhn-Tucker (KKT) system is first derived in the continuous functional analytic setting, followed by a consistent spatiotemporal discretization.

4.1 Variational Formulation and Adjoint Analysis

Let V' denote the topological dual of the energy space V with respect to the Hilbert space H, forming the standard Gelfand triple $V \hookrightarrow H \hookrightarrow V'$. Accordingly, we introduce the space of state trajectories with finite kinetic and potential energy:

$$\mathcal{W}(0,T) := \left\{ y \in L^2(0,T;V) \;\middle|\; y_t \in L^2(0,T;H),\ y_{tt} \in L^2(0,T;V') \right\}, \tag{33}$$

and denote the space of admissible controls by $\mathcal{U} := L^2(0,T;U)$.

Let $p(t)$ denote the adjoint state, identified as the Lagrange multiplier associated with the dynamic constraint (5). Under the standing assumptions and compatible terminal data, the adjoint state admits the regularity

$$p \in C([0,T];V) \cap C^1([0,T];H). \tag{34}$$

The Lagrangian functional $\mathcal{L} : \mathcal{W}(0,T) \times \mathcal{U} \times L^2(0,T;V) \to \mathbb{R}$ is defined by

$$\mathcal{L}(y,u,p) := J_T(y,u) + \int_0^T \langle y_{tt}(t) + A_0 y(t) - B_0 u(t), p(t) \rangle_{V',V}, \mathrm{d}t, \tag{35}$$

where $\langle \cdot, \cdot \rangle_{V',V}$ denotes the duality pairing between V' and V, which coincides with the inner product on the Hilbert space H whenever both arguments belong to H. $J_T(y,u)$ is the quadratic objective functional in the energy space, consistent with the model-specific functionals (9) (wave equation) and (13) (Timoshenko beam).

Stationarity of $\mathcal{L}$ with respect to y, u, and p (i.e., $\nabla \mathcal{L} = 0$), combined with standard integration by parts in time and space, yields the canonical coupled boundary value problem for the optimality system. This formulation preserves the infinite-dimensional structure and provides a rigorous basis for subsequent consistent discretization.

Theorem 2 (First-Order Optimality Conditions)**.** *Let the operator A_0 and the spaces H, V be defined as in Section 2. The optimal triple $(\hat{y}, \hat{u}, \hat{p})$ is uniquely characterized by the solution to the following coupled system:*

1. *State Equation (Forward in time):*

$$\begin{cases} \hat{y}_{tt}(t) + A_0 \hat{y}(t) = B_0 \hat{u}(t), & t \in (0,T), \\ \hat{y}(0) = y_0, \quad \hat{y}_t(0) = 0. \end{cases} \tag{36}$$

2. *Adjoint Equation (Backward in time):*

$$\begin{cases} \hat{p}_{tt}(t) + A_0 \hat{p}(t) = \hat{y}_{tt}(t) - A_0(\hat{y}(t) - y_d), & t \in (0,T), \\ \hat{p}(T) = 0, \quad \hat{p}_t(T) = \hat{y}_t(T). \end{cases} \tag{37}$$

   The adjoint equation is presented here in a second-order form consistent with the variational structure of the cost functional; equivalent formulations obtained by eliminating $\hat{y}_{tt}$ via the state equation are possible and lead to the same optimality system.

3. *Stationarity Condition:*

$$\gamma \hat{u}(t) - B_0^* \hat{p}(t) = 0 \quad \Longrightarrow \quad \hat{u}(t) = \frac{1}{\gamma} B_0^* \hat{p}(t), \quad t \in (0,T), \tag{38}$$

   where $B_0^* : H \to U$ denotes the Hilbert space adjoint of B_0.

The source term $-A_0(\hat{y} - y_d)$ in (37) corresponds to the Fréchet derivative of the potential energy term in the cost functional, and the terminal condition $\hat{p}_t(T) = \hat{y}_t(T)$ arises from the kinetic energy term.

Remark 4. *In the distributed control examples of Section 5, the control operator is the identity, $B_0 = I$. Consequently, the optimality condition simplifies to*

$$\hat{u}(t) = \frac{1}{\gamma} \hat{p}(t), \quad t \in (0,T),$$

allowing the control variable to be explicitly eliminated from the coupled state-adjoint system.

4.2 Numerical Discretization and Optimization Algorithm

The continuous optimality system is solved numerically using a conforming Finite Element Method (FEM) for spatial discretization and the implicit Newmark-β scheme for temporal integration. To distinguish physical turnpike decay from algorithmic damping, we employ a strategy that adapts the integration parameters based on the problem characteristics. The resulting discrete control problem is minimized via a Conjugate Gradient (CG) method applied to the reduced cost functional.

4.2.1 Spatiotemporal Discretization

Let $V_h \subset V$ be a finite-dimensional subspace spanned by the nodal basis functions $\{\phi_i\}_{i=1}^{N_h}$. The state y, adjoint p, and control u are approximated in this basis as:

$$y_h(t,x) = \sum_{i=1}^{N_h} Y_i(t)\phi_i(x),\ p_h(t,x) = \sum_{i=1}^{N_h} P_i(t)\phi_i(x),\ u_h(t,x) = \sum_{i=1}^{N_h} U_i(t)\phi_i(x), \tag{39}$$

where $Y(t), P(t), U(t) \in \mathbb{R}^{N_h}$ are the time-dependent nodal coefficient vectors:

$$Y(t) := [Y_1(t), \dots, Y_{N_h}(t)]^\top,$$

with analogous definitions for $P(t)$ and $U(t)$. Substituting the expansions (39) into the weak form of the state and adjoint equations leads to the semi-discrete system of ODEs:

$$\mathrm{M}\ddot{Y}(t) + \mathrm{K}Y(t) = F(t), \tag{40}$$

$$\mathrm{M}\ddot{P}(t) + \mathrm{K}P(t) = \mathrm{M}\ddot{Y}(t) - \mathrm{K}(Y(t) - Y_d), \tag{41}$$

where M and K are the standard mass and stiffness matrices:

$$\mathrm{M}_{ij} = \langle \phi_j, \phi_i \rangle_H, \quad \mathrm{K}_{ij} = \langle A_0^{1/2}\phi_j, A_0^{1/2}\phi_i \rangle_H.$$

The load vector $F(t)$ corresponds to the distributed control u_h:

$$F_i(t) = \int_\Omega u_h(t,x)\phi_i(x)\,dx = \sum_{j=1}^{N_h} U_j(t)M_{ij} \quad \Longrightarrow \quad F(t) = \mathrm{M}U(t). \tag{42}$$

This arises because the control enters linearly as a source term and is discretized in the same basis as the state. The time interval $[0,T]$ is divided into N_t uniform steps of size $\Delta t = T/N_t$. Applying the implicit Newmark-β scheme [16], the semi-discrete state equation (40) is advanced in time by solving the linear system:

$$(\mathrm{M} + \beta_N \Delta t^2 \mathrm{K})Y_{n+1} = \Delta t^2 \beta_N \mathrm{M}\boldsymbol{U}_{n+1} + \mathrm{M}\Big(Y_n + \Delta t \dot{Y}_n + \Delta t^2 \Big(\frac{1}{2} - \beta_N\Big)\ddot{Y}_n\Big), \tag{43}$$

with the corresponding updates for velocity $\dot{Y}_{n+1}$ and acceleration $\ddot{Y}_{n+1}$ using standard Newmark formulas. Regarding the choice of Newmark parameters (γ_N, β_N), we prioritize the symplectic (energy-conserving) trapezoidal rule ($\gamma_N = 1/2, \beta_N = 1/4$) for the verification of spectral decay rates. This ensures that the observed convergence is strictly driven by the optimal control feedback. For stiff coupled systems requiring high-frequency stabilization, appropriate numerical dissipation is introduced via modified parameters, as detailed in the specific numerical examples in Section 5.

The adjoint equation is integrated backward in time, from $t_{N_t} = T$ to $t_0 = 0$, using the same Newmark-β scheme and incorporating terminal conditions:

$$P_{N_t} = 0, \quad \dot{P}_{N_t} = \dot{Y}_{N_t}. \tag{44}$$

4.2.2 Numerical Optimization Strategy

The discrete optimization problem is addressed by minimizing the reduced cost functional $\hat{J}_h(U)$. Let $\mathcal{S}_h : U \mapsto Y(U)$ denote the discrete control-to-state operator, which maps a given control input to the unique solution of the forward problem (40). The reduced functional is defined by evaluating the objective functional on the manifold satisfying the state equation:

$$\hat{J}_h(U) := J_T(\mathcal{S}_h(U), U). \tag{45}$$

The minimization is performed via the Conjugate Gradient (CG) method applied to the reduced functional [23].

To ensure mesh-independent convergence behavior, gradients are computed with respect to the discrete $L^2(Q_T)$ inner product. This metric corresponds to the discrete inner product in $L^2(\Omega)$ induced by the finite element mass matrix M, ensuring consistency with the underlying Hilbert space geometry. For two space-time vectors U and V, this inner product is approximated using the trapezoidal quadrature rule in time:

$$\langle U, V \rangle_{L^2(Q_T)} \approx \Delta t \sum_{n=0}^{N_t} w_n \, U_n^\top \mathrm{M} \, V_n, \tag{46}$$

where w_n denote the quadrature weights given by $w_0 = w_{N_t} = 1/2$ and $w_n = 1$ for $1 \leq n \leq N_t - 1$. Under this inner product, the Riesz representative of the gradient, denoted by G, is identified as the coefficient vector

$$G_n = \nabla_U \hat{J}_h \big|_n = \gamma U_n - P_n, \quad n = 0, \ldots, N_t, \tag{47}$$

where P_n is the discrete adjoint vector satisfying (41). This vector G serves as the discrete gradient direction used to update the control in the CG iteration. The complete iterative optimization procedure is detailed in Algorithm 1.

Algorithm 1 Conjugate Gradient Method for $(OCP)_T$

Input: Initial discrete control $U^{(0)} = 0$, tolerance $\epsilon > 0$.
Output: Optimal discrete control U^*.

Step 1: Initialization
  Solve discrete state equation (40) with $U^{(0)}$ to obtain $Y^{(0)}$.
  Solve discrete adjoint equation (41) with $Y^{(0)}$ to obtain $P^{(0)}$.
  Compute initial gradient $G^{(0)} = \gamma U^{(0)} - P^{(0)}$.
  Set initial direction $D^{(0)} = -G^{(0)}$ and $k = 0$.
Step 2: Iterative Minimization
while $\|G^{(k)}\| > \epsilon$ **do**
    Determine step size α_k via Armijo backtracking.
    Update control: $U^{(k+1)} = U^{(k)} + \alpha_k D^{(k)}$.
    Gradient Evaluation:
      a) Solve discrete state Eq. (40) with $U^{(k+1)}$ to obtain $Y^{(k+1)}$.
      b) Solve discrete adjoint Eq. (41) with $Y^{(k+1)}$ to obtain $P^{(k+1)}$.
      c) Compute gradient: $G^{(k+1)} = \gamma U^{(k+1)} - P^{(k+1)}$.
    Conjugate Direction Update (Fletcher-Reeves):
      Compute $\beta_k = \frac{\langle G^{(k+1)}, G^{(k+1)} \rangle}{\langle G^{(k)}, G^{(k)} \rangle}$.
      Update direction: $D^{(k+1)} = -G^{(k+1)} + \beta_k D^{(k)}$.
      Set $k = k + 1$.
end while

5 Numerical Results

This section provides a quantitative verification of the asymptotic behavior established in Theorem 1. The objective is to quantify the pointwise discrepancy between the finite-horizon optimal state y_T and the theoretically constructed *Initial Limit Arc* Ξ, representing the unique infinite-horizon optimal trajectory. Particular emphasis is placed on verifying the spectral dichotomy predicted by Theorem 1, namely the decomposition of the error dynamics into a control-dominated oscillatory component and a saturation-limited monotone component, governed by the interaction between the regularization parameter γ and the principal (lowest) eigenvalue of the operator.

The discretized optimal control problems are solved using the adjoint-based Conjugate Gradient scheme described in Algorithm 1. All spatial discretizations are implemented using conforming finite element spaces provided by FEniCSx (DolfinX, version 0.10.0) [22]. To distinguish the asymptotic convergence of the optimal feedback from spurious numerical dissipation, the time integration scheme is adapted to the problem regularity: the symplectic trapezoidal rule is employed for the wave equation benchmarks to ensure exact

discrete energy conservation, whereas for the stiff Timoshenko beam system, the Newmark-β scheme with dissipative parameters is employed to stabilize high-frequency modes.

Three representative benchmark problems are considered: (i) the 1D wave equation serving as a spectral reference; (ii) the 2D wave equation on the unit square illustrating multidimensional spectral effects; and (iii) the Timoshenko beam system demonstrating the applicability of the theoretical framework to coupled vector-valued dynamics. In all cases, the desired state is the zero equilibrium, $y_d \equiv 0$, consistent with the formulation in Section 2.

5.1 Case 1: 1D Wave Equation on the Unit Interva

We begin with the 1D wave equation on the unit interval $\Omega = (0, 1)$, where $A_0 = -\partial_{xx}$ denotes the Dirichlet Laplacian. Since the analytic eigenvalues are explicitly given by $\lambda_j = (j\pi)^2$ for $j \in \mathbb{N}$, making this case an ideal spectral benchmark for validating the theoretical decay rates. The spatial domain is discretized using a uniform finite element mesh with grid size $h = 1/50$, , employing the finite element space $V_h \subset H_0^1(\Omega)$ spanned by piecewise linear Lagrange basis functions. The time interval is partitioned with a fixed time step $\Delta t = 0.01$. To rigorously isolate the control-induced spectral behavior from algorithmic dissipation, the temporal integration is performed using the symplectic trapezoidal rule (Newmark parameters $\gamma_N = 0.5, \beta_N = 0.25$). This choice ensures that the discrete energy of the unforced system is conserved, so that any observed asymptotic decay is strictly attributable to the optimal control feedback. The discrete optimization is solved via Algorithm 1 with a gradient norm tolerance $\epsilon = 10^{-8}$.

To verify the spectral dichotomy, we initialize the system with the fundamental eigenmode for both regimes: $y_0(x) = \sin(\pi x)$. This choice excites the lowest spectral mode, which is predicted to govern the asymptotic decay rate. We measure the trajectory discrepancy at a fixed observation time $t_{obs} = 0.02$ using the $L^2(\Omega)$-norm:

$$E_H(T) := \|y_T(t_{obs}) - \Xi(t_{obs})\|_H = \left(\int_0^1 |y_T(t_{obs}, x) - \Xi(t_{obs}, x)|^2 \, \mathrm{d}x \right)^{1/2}. \tag{48}$$

Although Theorem 1 establishes convergence in the stronger energy topology V, the continuous embedding $V \hookrightarrow H$ implies that $E_H(T)$ decays exponentially at the same spectral rate.

Since the exact Initial Limit Arc $\Xi(t)$ is defined on an infinite horizon, it is numerically approximated by a finite-horizon solution $y_{T_{ref}}(t)$ computed with a sufficiently large horizon $T_{ref} \gg t_{obs}$. According to the exponential convergence property established in Theorem 1, the approximation error at the observation time t_{obs} is bounded by:

$$\left\| \Xi(t_{obs}) - y_{T_{ref}}(t_{obs}) \right\|_V \leq C \, \|y_0\|_V \, e^{-\mu(T_{ref} - t_{obs})}. \tag{49}$$

Given that $t_{obs} = 0.02$ and $T_{ref} = 100$, and considering the spectral gap $\mu > 0$, this truncation error scales as $\mathcal{O}(e^{-\mu T_{ref}})$, which is numerically negligible compared to the discretization error. Thus, $y_{T_{ref}}$ serves as a valid surrogate for the true limit Ξ.

Regime I: Oscillatory Convergence ($\gamma = 1$). We first investigate the oscillatory regime by setting $\gamma = 1$. The fundamental eigenvalue is $\lambda_1 = \pi^2 \approx 9.87 > (8\gamma)^{-1} = 0.125$. The spectral analysis predicts oscillatory convergence with decay rate $\mu = \frac{1}{2\sqrt{\gamma}} = 0.5$. The evolution of the finite-horizon optimal state y_T and control u_T is displayed in Fig. 1 and Fig. 2 for time horizons $T \in \{1, 10, 100\}$. As T increases, the initial segment of each trajectory progressively aligns with the Initial Limit Arc Ξ, stabilizing onto the turnpike structure. The quantitative error analysis in Fig. 3 (left) confirming the exponential nature of the convergence. The logarithmic plot of the L^2-error exhibits a strict linear trend. Crucially, the empirical decay is significantly faster than the theoretical lower bound (represented by the red dashed line). Since the numerical scheme is energy-conserving, this rapid convergence confirms that the theoretical estimate provides a valid, albeit conservative, lower bound on the true spectral decay. Fig. 3 (right) illustrates the stabilization of the state profile $y_T(t, x_c)$ at the midpoint $x_c = 0.5$. As the time horizon T extends, the finite-horizon trajectories rapidly synchronize with this unique reference trajectory (black dashed line) during the initial transient phase, visually confirming the turnpike property in the pointwise sense.

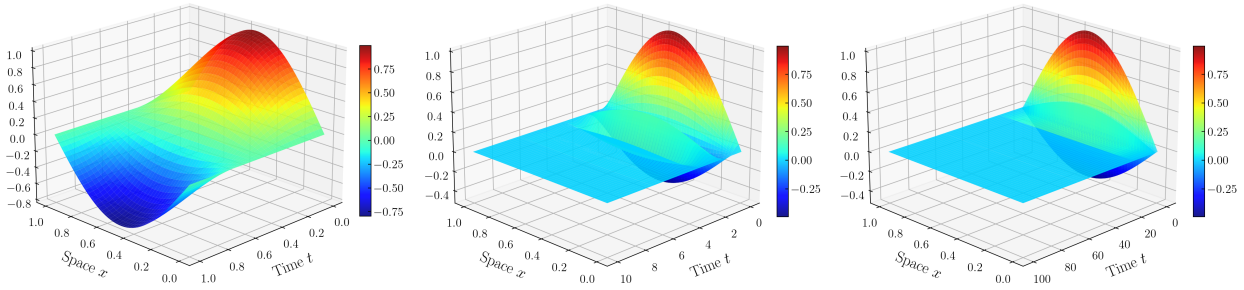

Figure 1: Evolution of the optimal state $y_T(t,x)$ for time horizons $T \in \{1, 10, 100\}$ in the 1D wave equation (oscillatory regime).

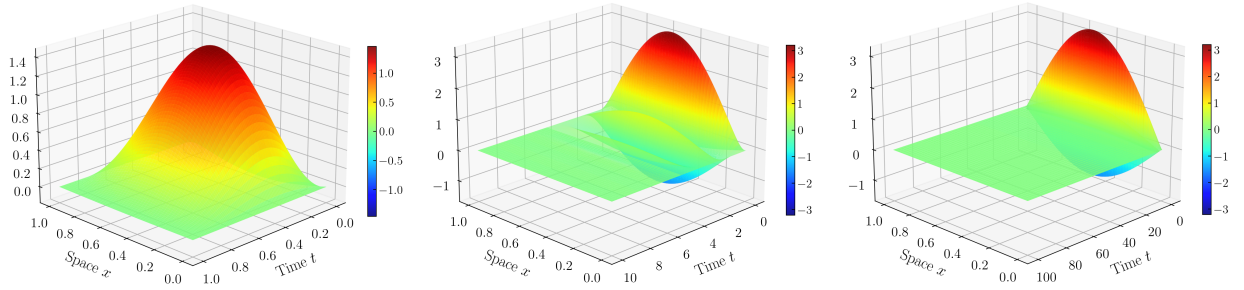

Figure 2: Evolution of the optimal control $u_T(t,x)$ for time horizons $T \in \{1, 10, 100\}$ in the 1D wave equation (oscillatory regime).

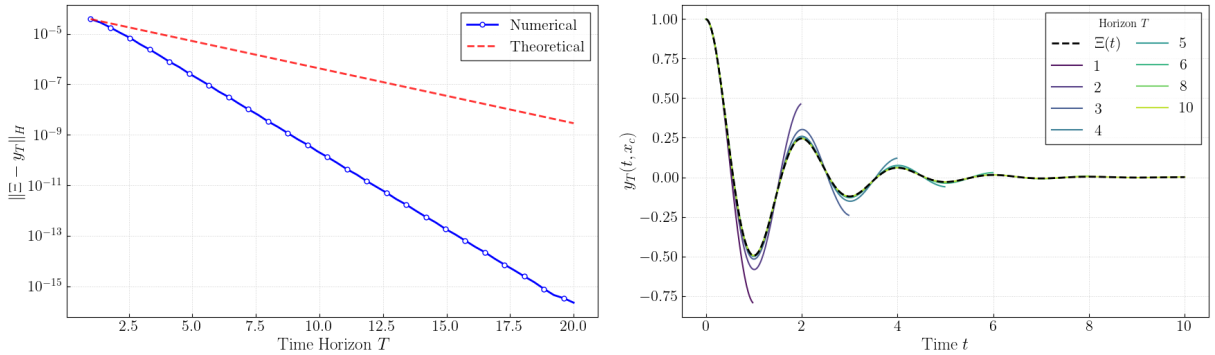

Figure 3: Oscillatory regime behavior for the 1D wave equation ($\gamma = 1$). Left: Global L^2-error $\|y_T(t_{\text{obs}}) - \Xi(t_{\text{obs}})\|_H$ at $t_{\text{obs}} = 0.02$ versus the time horizon T (semilog scale). Right: Temporal profiles of the state $y_T(t, x_c)$ at $x_c = 0.5$ for various horizons T.

Regime II: Monotonic Convergence ($\gamma = 10^{-3}$). We now consider a much smaller regularization parameter, $\gamma = 10^{-3}$. In this regime, the fundamental eigenvalue satisfies $\lambda_1 = \pi^2 < (8\gamma)^{-1} = 125$, indicating that the system operates in the monotonic (overdamped) regime. Although the control-dependent rate $\frac{1}{2\sqrt{\gamma}} \approx 15.8$ predicts a very rapid decay, Theorem 1 shows that the convergence is ultimately limited by the system's intrinsic dynamics, which impose a maximum decay rate of $\mu = \text{Re}(\sqrt{\lambda_1}) = \pi \approx 3.14$.

The numerical results in Fig. 4 provide clear evidence of this saturation effect. In Fig. 4 (left), the empirical error decay (blue solid line) is compared with the control-predicted rate (green dotted line) and the intrinsic spectral limit (red dashed line). The error initially follows the steep control-predicted rate but asymptotically aligns with the spectral limit $\sqrt{\lambda_1}$, confirming that as $\gamma \to 0$, the turnpike convergence rate is ultimately constrained by the real parts of the open-loop characteristic roots. The state evolution in Fig. 4 (right) shows strictly monotonic convergence to the limit arc, in contrast to the oscillatory behavior observed

in Regime I, consistent with the bifurcation of the characteristic roots from the complex plane to the real axis.

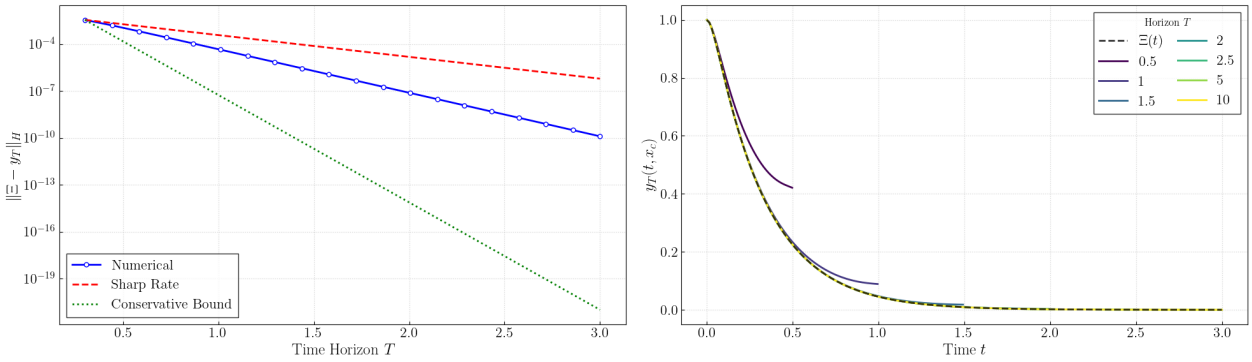

Figure 4: Monotonic regime behavior for the 1D wave equation ($\gamma = 0.001$). Left: Global L^2-error $\|y_T(t_{obs}) - \Xi(t_{obs})\|_H$ at $t_{obs} = 0.02$ versus time horizon T (semilog scale). Right: Temporal profiles of the state $y_T(t, x_c)$ at $x_c = 0.5$ for various horizons T.

5.2 Case 2: 2D Wave Equation on the Unit Square

We extend the validation to the two-dimensional setting by considering the wave equation on the unit square $\Omega = (0, 1)^2$. The operator $A_0 = -\Delta$ is equipped with homogeneous Dirichlet boundary conditions. The spectrum is given explicitly by $\lambda_{k,m} = \pi^2(k^2 + m^2)$ for $k, m \in \mathbb{N}$. We initialize the system with the principal eigenmode $y_0(x) = \sin(\pi x_1)\sin(\pi x_2)$, associated with the lowest eigenvalue $\lambda_{1,1} = 2\pi^2 \approx 19.74$.

To ensure high spatial accuracy, the domain is discretized using a structured triangular mesh with characteristic length $h = 1/32$, employing quadratic Lagrange finite elements (P_2) for both the state and control variables. Consistent with the 1D benchmark, temporal integration utilizes the symplectic trapezoidal rule ($\gamma_N = 0.5, \beta_N = 0.25$) with a time step $\Delta t = 0.01$. This choice eliminates numerical dissipation, ensuring that the observed error dynamics are driven solely by the optimal control optimality system. We set the regularization parameter to $\gamma = 1$. Since the principal eigenvalue satisfies $\lambda_{1,1} \approx 19.74 \gg (8\gamma)^{-1} = 0.125$, the system operates deeply within the oscillatory regime. Theorem 1 predicts a global exponential decay rate dominated by the control term: $\mu \geq \frac{1}{2\sqrt{\gamma}} = 0.5$. The Initial Limit Arc $\Xi(t)$ is approximated using a reference trajectory computed over a long horizon $T_{ref} = 20$.

The numerical results presented in Fig. 5 provide quantitative verification of these estimates in the multidimensional context. The global discrepancy $E_H(T)$ (Fig. 5, left) exhibits a characteristic linear profile on the semi-logarithmic scale. The empirical decay rate closely tracks the theoretical prediction of $\mu = 0.5$. Correspondingly, the state trajectory evaluated at the domain center $x_c = (0.5, 0.5)$ (Fig. 5, right) demonstrates pointwise convergence to the Initial Limit Arc $\Xi(t, x_c)$. As the horizon T increases, the finite-horizon solutions progressively coincide with the limit trajectory, numerically verifying the dynamic turnpike property for multidimensional spectra.

5.3 Case 3: Timoshenko Beam Control

This final benchmark addresses the clamped-clamped Timoshenko beam, a coupled hyperbolic system governing the vertical displacement $w(t, x)$ and the rotation angle $\varphi(t, x)$ in (10). This case validates the framework's applicability to vector-valued dynamics. We consider a steel beam of length $L = 1\,\text{m}$ with Young's modulus $E = 200\,\text{GPa}$, density $\rho = 7800\,\text{kg/m}^3$, and shear correction factor $\kappa_s = 5/6$. The derived operator parameters are $I_\rho = 6.50 \times 10^{-6}\,\text{kg} \cdot \text{m}$ and $K = 6.41 \times 10^6\,\text{N}$. The beam is subject to homogeneous Dirichlet boundary conditions at both ends, physically corresponding to a clamped-clamped configuration where both vertical displacement and rotation are fixed to zero ($w = \varphi = 0$ at $x \in \{0, L\}$). The system is initialized from

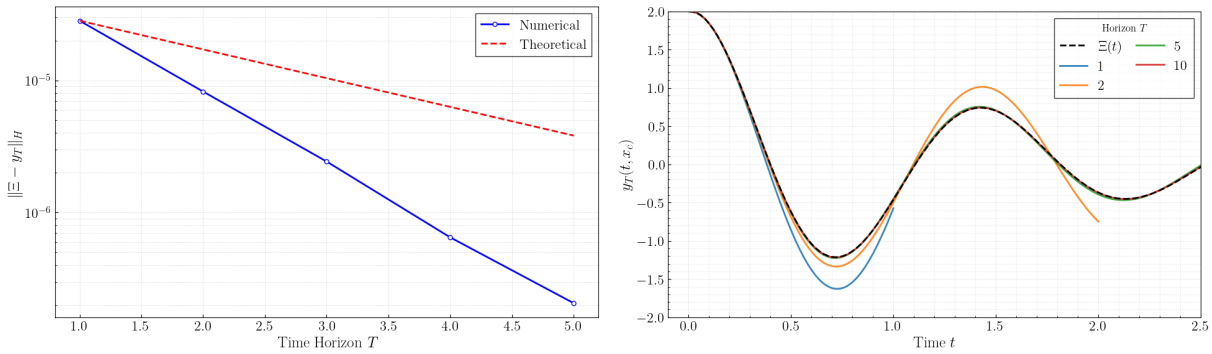

Figure 5: Numerical illustration for the 2D wave equation ($\gamma = 1$). Left: Global L^2-error $\|y_T(t_{\text{obs}}) - \Xi(t_{\text{obs}})\|_H$ at $t_{\text{obs}} = 0.02$ versus the time horizon T (semilog scale). Right: Temporal profiles of the state $y_T(t, x_c)$ at the domain center $x_c = (0.5, 0.5)$ for various horizons T.

rest ($\partial_t \boldsymbol{y}(0, x) = \mathbf{0}$) with a prescribed initial displacement profile:

$$w(0, x) = 2 \times 10^{-3} \left(1 - \cos\left(\frac{2\pi x}{L}\right)\right), \quad \varphi(0, x) = 0. \tag{50}$$

The physical configuration is illustrated in Fig. 6.

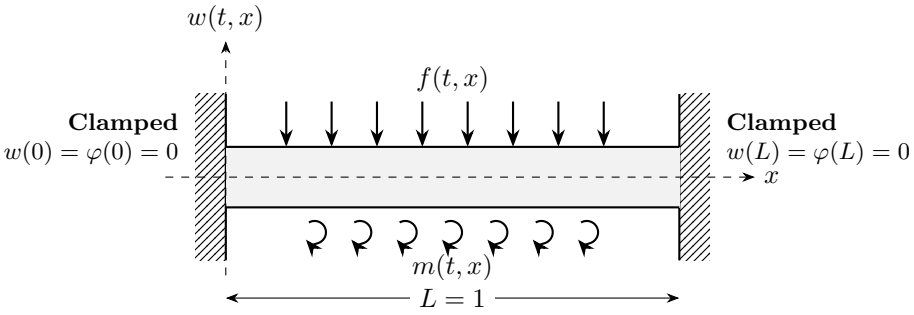

Figure 6: Illustration of a clamped-clamped Timoshenko beam with distributed force $f(t, x)$ and moment $m(t, x)$.

The regularization parameter is set to $\gamma = 0.1$. The spatial domain is discretized using linear Lagrange finite elements (P_1) on a uniform mesh with $N_e = 50$ elements. Unlike the scalar wave equation, the coupled Timoshenko system admits stiff shear modes prone to high-frequency numerical oscillations. To ensure stability, we employ the dissipative Newmark scheme with parameters $\gamma_N = 0.6$, $\beta_N = 0.3025$ and $\Delta t = 0.002$. This parameter choice introduces necessary algorithmic damping to stabilize the discrete spectrum while maintaining second-order accuracy for low-frequency modes.

The Initial Limit Arc $\Xi(t)$ is approximated using a reference trajectory computed over a horizon $T_{\text{ref}} = 20$. Given the coupled displacement-rotation dynamics, convergence is quantified in the global energy norm $\|\cdot\|_{\mathcal{X}}$ defined in Eq. (6), rather than the scalar L^2-metric employed for the 1D and 2D wave cases. The quantitative results are summarized in Fig. 7. The energy-based error exhibits strict exponential decay (Fig. 7, left). Notably, the empirical decay rate exceeds the theoretical control-induced lower bound $\mu \geq 1/(2\sqrt{\gamma})$, reflecting the additional damping introduced by the time integration scheme, which stabilizes high-frequency shear modes. Correspondingly, the vertical displacement trajectory $w_T(t, 0.5)$ (Fig. 7, right) demonstrates pointwise convergence to the limit profile $\Xi(t)$.

The vector-valued turnpike property is further illustrated in Fig. 8, showing the temporal evolution of the optimal control components $f_T(t, 0.5)$ and $m_T(t, 0.5)$. For short horizons ($T = 0.5$, left), the controls are dominated by the transient effort required to steer the system. As the horizon is extended to $T = 1.0$ (right), a clear structural transition emerges: after the initial transient phase ($t > 0.6$), both controls decay

and stabilize near the steady-state values u_d. This behavior explicitly confirms the static turnpike property: for sufficiently long horizons, the dynamic optimization problem recovers the steady-state optimality, where the control effort remains approximately constant to maintain the system at the desired equilibrium.

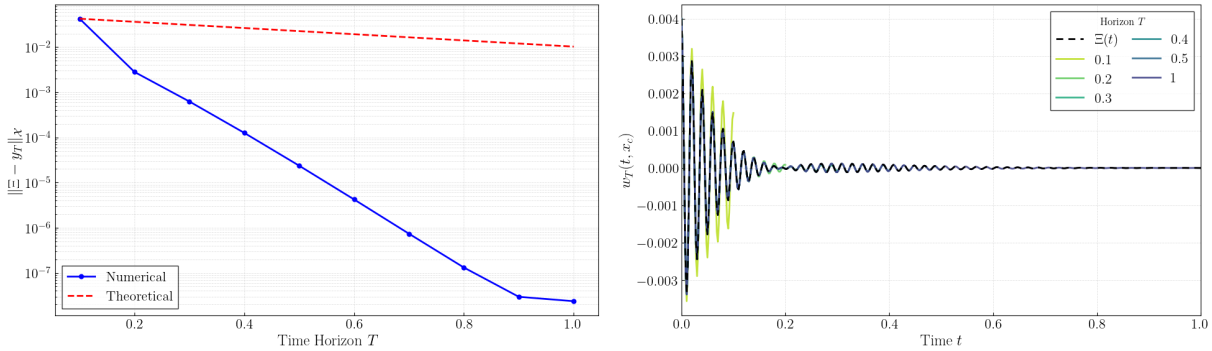

Figure 7: Numerical illustration of convergence in the energy norm for the Timoshenko beam model ($\gamma = 0.1$). Left: Global error $\|\Xi - y_T\|_{\mathcal{X}}$ in the energy space at $t_{\text{obs}} = 0.02$ versus the time horizon T (semilog scale). Right: Temporal profiles of the vertical displacement $w_T(t, x_c)$ at the midpoint $x_c = 0.5$ for various horizons T.

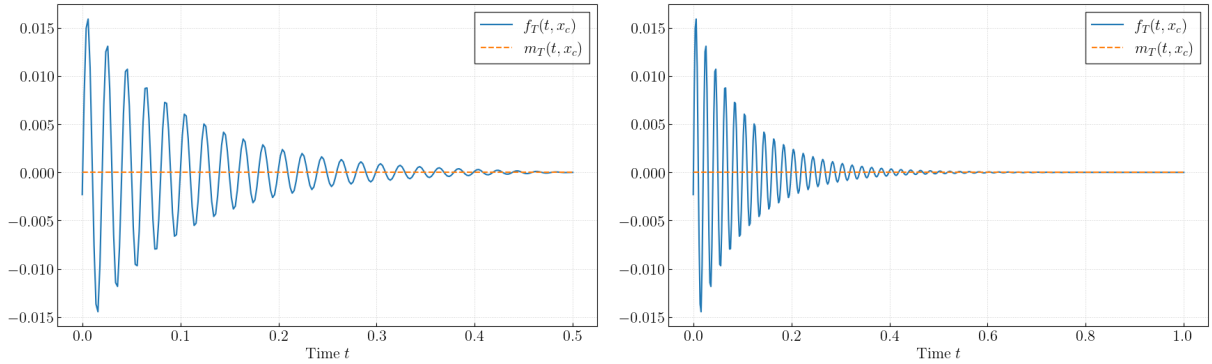

Figure 8: Optimal distributed controls $f_T(t, x_c)$ and $m_T(t, x_c)$ at $x_c = 0.5$ for time horizon $T = 0.5$ (left) and $T = 1$ (right).

6 Conclusions

The primary contribution of this work is a rigorous spectral characterization of transient optimal trajectories for abstract second-order evolution equations. We introduced the *Initial Limit Arc*, proving that it coincides with the unique infinite-horizon optimal trajectory evolving on the stable invariant manifold. Unlike classical static turnpike theory, this dynamic construct captures the transient phase. We established that finite-horizon optimal states converge to this limit uniformly in the energy norm, with error dynamics governed strictly by the spectral gap of the underlying Hamiltonian operator.

A key finding is the spectral bifurcation of the convergence mechanism based on the control cost—specifically, the sharp transition from a control-dominated oscillatory regime to a saturation-limited monotonic regime. Numerical validation on the wave equation and the Timoshenko beam confirms this structure. Crucially, the empirical decay rates consistently satisfy the theoretical lower bounds and validate the sharpness of the spectral estimate in the conservative limit. The use of symplectic integrators further ensures that these observations reflect physical control authority rather than algorithmic dissipation.

While the current framework relies on discrete spectral decomposition, it lays the groundwork for broader extensions. Future research will address systems with continuous spectra, semilinear dynamics, and boundary

control with unbounded operators. Additionally, investigating the impact of uncertainty in random hyperbolic systems remains a relevant direction for robust control design [13].

Finally, this analysis bridges dynamic control theory and geometric design. Optimal design of distributed-parameter systems is well-established in the static setting, employing topological [28, 24, 29, 30] and shape derivatives [26]. However, the justification for applying these static tools to evolutionary problems has traditionally been heuristic. The asymptotic stability established here provides the missing theoretical foundation: since the dynamic optimal trajectory converges exponentially to the steady state, the infinite-horizon cost is dominated by the static performance. This justifies the use of static shape optimization as a rigorous proxy for long-term dynamic design in flexible mechanical systems (see [28]).

A Explicit Derivations and Asymptotic Analysis

In this appendix, we provide the explicit construction of the finite-horizon optimal solutions and the rigorous derivation of their infinite-horizon limits, as utilized in the proof of Theorem 1.

A.1 Explicit Solution for the Oscillatory Regime ($j \in I_{osc}$)

The characteristic roots are complex with $\lambda_j > \frac{1}{8\gamma}$. Let ω_j denote the stable root with $\mathrm{Re}(\omega_j) < 0$. The roots satisfy the properties:

$$|\omega_j|^4 = \lambda_j(\lambda_j + \gamma^{-1}), \quad \mathrm{Re}(\omega_j^2) = -(\lambda_j - (2\gamma)^{-1}). \tag{51}$$

The optimal coefficient $\alpha_j(T;t)$ satisfying the boundary value problem is given by:

$$\begin{aligned}\alpha_j(T;t) = A_j(T)\left[(\bar{\omega}_j^2 + \lambda_j)\cosh(\omega_j(T-t)) - (\omega_j^2 + \lambda_j)\cosh(\bar{\omega}_j(T-t))\right] \\ + B_j(T)\Big[\bar{\omega}_j\left(\bar{\omega}_j^2 + \lambda_j - \gamma^{-1}\right)\sinh(\omega_j(T-t)) \\ - \omega_j\left(\omega_j^2 + \lambda_j - \gamma^{-1}\right)\sinh(\bar{\omega}_j(T-t))\Big].\end{aligned} \tag{52}$$

The coefficients $A_j(T)$ and $B_j(T)$ are derived from the terminal conditions at $t = T$:

$$A_j(T) = -\frac{\eta_j}{N_j(T)}|\omega_j|^2\left[\left(\bar{\omega}_j^2 + \lambda_j - \gamma^{-1}\right)\cosh(\omega_j T) - \left(\omega_j^2 + \lambda_j - \gamma^{-1}\right)\cosh(\bar{\omega}_j T)\right], \tag{53}$$

$$B_j(T) = -\frac{\eta_j}{N_j(T)}\left[-\omega_j(\bar{\omega}_j^2 + \lambda_j)\sinh(\omega_j T) + \bar{\omega}_j(\omega_j^2 + \lambda_j)\sinh(\bar{\omega}_j T)\right], \tag{54}$$

where the common denominator is:

$$N_j(T) = |\omega_j|^2\left[\frac{4\lambda_j}{\gamma} + \left(\frac{4\lambda_j}{\gamma} - \gamma^{-2}\right)|\cosh(\omega_j T)|^2\right] + \lambda_j\left(\frac{4\lambda_j}{\gamma} + \gamma^{-2}\right)|\sinh(\omega_j T)|^2. \tag{55}$$

A.2 Derivation of the Modal Error Bound

We analyze the pointwise error $e_j(T;t) := \alpha_j(T;t) - \Xi_j(t)$ for a fixed mode j. Since both α_j and Ξ_j satisfy the same fourth-order ODE, the error e_j is a solution to the homogeneous equation. However, unlike Ξ_j, which satisfies the stability condition at infinity, e_j is driven by the mismatch at the terminal time T.

The terminal value of the limit arc is $\Xi_j(T) = \eta_j L_j(T)$. Since $L_j(t)$ decays exponentially, the boundary condition mismatch scales as:

$$|\Xi_j(T)| \approx C|\eta_j|e^{-\mu T}. \tag{56}$$

This terminal residual acts as a boundary source term that excites the unstable modes (associated with roots $-\omega_j, -\bar{\omega}_j$) in the backward time direction. The propagation of this error from T back to t scales as $e^{-\mu(t-T)}$. Consequently, the magnitude of the error at time t is bounded by:

$$|\alpha_j(T;t) - \Xi_j(t)| \le K|\Xi_j(T)| \cdot e^{\mu(t-T)} \le K'|\eta_j|e^{-\mu T}e^{\mu(t-T)} = K'|\eta_j|e^{-\mu(T-t)}. \tag{57}$$

This uniform estimate justifies the modal bound utilized in Step 4 of the main proof.

Acknowledgements

This work was supported by Deutsche Forschungsgemeinschaft (DFG) in the Collaborative Research Centre CRC/Transregio 154, Mathematical Modelling, Simulation and Optimization Using the Example of Gas Networks, Projects C03 and C05, Projektnummer 239904186.

References

[1] J.M. Ball, J.E. Marsden, and M. Slemrod. Feedback control in an infinite-dimensional system. *SIAM J. Control Optim.*, 20(4):600–629, 1982.

[2] C. Bardos, G. Lebeau, and J. Rauch. Sharp sufficient conditions for the observation, control, and stabilization of waves from the boundary. *SIAM J. Control Optim.*, 30(5):1024–1065, 1992.

[3] L. Bociu and J.-P. Zolésio. A pseudo-extractor approach to hidden boundary regularity for the wave equation with mixed boundary conditions. *J. Differ. Equ*, 259(11):5688–5708, 2015.

[4] J.-M. Coron. *Control and Nonlinearity*, volume 136. American Mathematical Society, Providence, RI, 2007.

[5] R. F. Curtain and H. Zwart. *An Introduction to Infinite-Dimensional Linear Systems Theory*. Springer New York, New York, NY, 1 edition, 1995.

[6] K. Datchev and P. Kleinhenz. Sharp polynomial decay rates for the damped wave equation with Hölder-like damping. *Proc. Amer. Math. Soc.*, 148(8):3417–3425, 2020.

[7] E. B. Davies. *Linear Operators and their Spectra*. Cambridge Univ. Press, 2007.

[8] K.-J. Engel and R. Nagel. *One-Parameter Semigroups for Linear Evolution Equations*. Springer, 2000.

[9] Timm Faulwasser and Lars Grüne. Turnpike properties in optimal control: An overview of discrete-time and continuous-time results. In *Handbook of Numerical Analysis*, volume 23, pages 367–400. Elsevier, 2022.

[10] L. Grüne and L. Krügel. Local turnpike analysis using local dissipativity for discrete time discounted optimal control. *Appl. Math. Optim.*, 84:1585–1606, 2021.

[11] L. Grüne and M. Stieler. Asymptotic stability and transient optimality of economic mpc without terminal conditions. *J. Process Control*, 24(8):1187–1196, 2014.

[12] M. Gugat and F. Hante. On the turnpike phenomenon for optimal boundary control problems with hyperbolic systems. *SIAM J. Control Optim.*, 57(2):941–965, 2019.

[13] M. Gugat and M. Herty. Turnpike properties of optimal boundary control problems with random linear hyperbolic systems. *ESAIM: Control Optim. Calc. Var.*, 29:55, 2023.

[14] M. Gugat, M. Herty, and C. Segala. The turnpike property for mean-field optimal control problems. *Eur. J. Appl. Math.*, 35(6):733–747, 2024.

[15] M. Gugat and J. Sokolowski. An aspect of the turnpike property. long time horizon behavior. *Serdica Math. J.*, 49(1–3), November 2023.

[16] Thomas J. R. Hughes. *The Finite Element Method: Linear Static and Dynamic Finite Element Analysis*. Prentice-Hall, 1987.

[17] J. U. Kim and Y. Renardy. Boundary control of the Timoshenko beam. *SIAM J. Control Optim.*, 25(6), 1987.

[18] I. Lasiecka and R. Triggiani. Riccati equations for hyperbolic partial differential equations with $L_2(0,t;L_2(\gamma))$—dirichlet boundary terms. *SIAM J. Control Optim.*, 24(5):884–925, 1986.

[19] C. Laurent and M. Léautaud. Observability of the heat equation, geometric constants in control theory, and a conjecture of Luc Miller. *Anal. PDE*, 14(2):355–423, 2021.

[20] J.-L. Lions. *Optimal Control of Systems Governed by Partial Differential Equations*. Springer Berlin Heidelberg, Berlin, Heidelberg, 1971.

[21] J.-L. Lions. *Exact Controllability, Stabilization and Perturbations of Distributed Systems*. SIAM, Philadelphia, PA, 1988.

[22] A. Logg and G. N. Wells. Dolfin: Automated finite element computing. *ACM Trans. Math. Softw.*, 37(2):1–28, 2010.

[23] J. Nocedal and S. J. Wright. *Numerical Optimization*. Springer Series in Operations Research and Financial Engineering. Springer, New York, NY, 2 edition, 2006.

[24] N. Osmolovskii, M. Qian, and J. Sokołowski. *Topological Derivative Method for the Optimum Design of Networks*, volume 82 of *Badania Systemowe*. Instytut Badań Systemowych PAN, Warsaw, 2025.

[25] A. Pazy. *Semigroups of Linear Operators and Applications to Partial Differential Equations*. Springer, New York, NY, 1983.

[26] P. I. Plotnikov and J. Sokołowski. Geometric aspects of shape optimization. *J. Geom. Anal.*, 33:206, 2023.

[27] A. Porretta and E. Zuazua. Long time versus steady state optimal control. *SIAM J. Control Optim.*, 51(6), 2013.

[28] M. Qian, J. R. de Faria, A. J. B. Santos, J. Sokołowski, and A. P. Wyse. Topological derivative method for design and control of Timoshenko beam networks. *Appl. Math. Optim.*, 2025. in press.

[29] M. Schuster and J. Sokołowski. The topological derivative method for optimum shape design and control of gas networks. *J. Appl. Numer. Optim.*, 7(3):309–332, 2025.

[30] J. Sokołowski and Y. Tan. Shape and topology optimization of control problems in elasticity. *Res. Math. Sci.*, 12(2):Paper No. 35, 22, 2025.

[31] O. J. Staffans. *Well-Posed Linear Systems*, volume 103 of *Cambridge Studies in Advanced Mathematics*. Cambridge University Press, Cambridge, 2005.

[32] E. Trélat, X. Zeng, and C. Zhang. The exponential turnpike property for periodic linear quadratic optimal control problems in infinite dimension. *SIAM J. Control Optim.*, 63(4), 2025.

[33] E. Trélat and C. Zhang. Integral and measure-turnpike properties for infinite-dimensional optimal control systems. *Math. Control Signals Syst.*, 30(3), 2018.

[34] E. Trélat and E. Zuazua. The turnpike property in finite-dimensional nonlinear optimal control. *J. Differ. Equ.*, 258(1):81–114, 2015.

[35] M. Tucsnak and G. Weiss. *Observation and Control for Operator Semigroups*. Birkhäuser Basel, Basel, 2009.

[36] A. J. Zaslavski. *Turnpike Properties in the Calculus of Variations and Optimal Control*. Springer, New York, NY, 2006.